nature physics

Perspective

https://doi.org/10.1038/s41567-026-03229-z

Loop-current order in kagome metals

Received: 10 February 2025

Accepted: 25 February 2026

Published online: 16 April 2026

Check for updates

Rafael M. Fernandes [1,2] ✉, Turan Birol [3] ✉, Mengxing Ye [4] ✉ & David Vanderbilt [5,6] ✉

Loop-current states arise when interacting electronic degrees of freedom collectively generate interatomic currents, producing a rare form of magnetic order in which spin does not play the primary role. The recent proposal of loop-current states in kagome superconductors has stimulated renewed interest in this exotic type of magnetism. We provide an overview of the phenomenological and symmetry properties of loop currents, as well as relevant microscopic models and ab initio methods in kagome materials. We then discuss how loop-current order generates a spin density wave through spin–orbit coupling and a charge density wave through anharmonic couplings present in systems with three-fold rotational symmetry. We briefly discuss the current status of loop-current order in kagome metals and open challenges, including their experimental detection and interplay with other orders such as superconductivity.

Magnetism is a phenomenon most commonly associated with the spin degrees of freedom and driven by exchange interactions. It is characterized by the spontaneous breaking of time-reversal symmetry, which relates magnetic moments pointing in opposite directions. Depending on the type of magnetic order, time-reversal-symmetry breaking (TRSB) can occur in combination with other broken symmetries, such as translation or rotation. Magnetic order can either have the same periodicity as the primitive cell or arise at a non-zero wavevector $\mathbf{Q}$ that breaks the periodicity, resulting in a spatial modulation of the electronic spin density called a spin density wave (SDW). In either case, the spin moments induce an orbital moment through spin–orbit coupling. However, the orbital moments are generally weak and localized within an atomic sphere because of quenching by the crystal field. Thus, in almost all known cases, the magnetic instability occurs in the spin sector.

However, it is also possible for a magnetic instability to occur directly in the orbital sector. Because of the quenching, this is unlikely to mimic the on-site circulating currents associated with orbital moments induced by spin–orbit coupling. Instead, interest has focused on so-called loop-current (LC) or flux states that are characterized by interatomic currents flowing between atoms[1–5]. In this case, the magnetism arises in the orbital sector (here 'orbital' refers to the spatial character of the electronic wavefunctions, not to atomic orbitals). Spin–orbit coupling can then induce spin moments on atomic sites, but these incidental moments are not responsible for the magnetic instability.

The potential mechanisms behind the LCs are a matter of active research. In the absence of broken time-reversal symmetry, the electronic wavefunction can be taken as real, so that the local current density vanishes everywhere. A phase prefactor multiplied by this wavefunction generates a current proportional to the gradient of this phase. This imposes a kinetic energy cost, proportional to the squared phase gradient, with no obvious energy gain. Theoretical models of LC states typically invoke specific mechanisms such as intersite, intervalley, or interpatch interactions to explain this magnetic instability.

Loop-current order can also lead to more exotic states of matter, such as an anomalous quantum Hall state[6], by which the system acquires a quantized Hall conductance of topological origin in the absence of an external magnetic field. The question of whether LC magnetic states are realized in materials has been discussed in diverse systems from cuprates[2,7] to colossal magnetoresistance materials[8]. More recently there has been a surge of research activity on this front, motivated partly by experimental discoveries related to the AV_3Sb_5 kagome metals (where A = Cs, K, Rb)[9,10], including a possible TRSB charge order[11] that can also coexist with superconductivity.

[1]Department of Physics, The Grainger College of Engineering, University of Illinois Urbana-Champaign, Urbana, IL, USA. [2]Anthony J. Leggett Institute for Condensed Matter Theory, The Grainger College of Engineering, University of Illinois Urbana-Champaign, Urbana, IL, USA. [3]Department of Chemical Engineering and Materials Science, University of Minnesota, Minneapolis, MN, USA. [4]Department of Physics and Astronomy, University of Utah, Salt Lake City, UT, USA. [5]Department of Physics and Astronomy, Rutgers University, Piscataway, NJ, USA. [6]Center for Materials Theory, Rutgers University, Piscataway, NJ, USA. ✉e-mail: rafaelf@illinois.edu; tbirol@umn.edu; mengxing.ye@utah.edu; dhv@physics.rutgers.edu

https://doi.org/10.1038/s41567-026-03229-z

BOX 1

Microscopic definitions of the LC and SDW order parameters

Consider a simple model of electrons hopping on the sites of a lattice. We introduce the N-dimensional spinor $\Psi_{\mathbf{k},s} = \left(\psi^{(\mu_1)}_{\mathbf{k},s}, \cdots, \psi^{(\mu_N)}_{\mathbf{k},s}\right)^{\mathrm{T}}$, where μ_i labels an internal degree of freedom (orbital or sublattice) and $\psi^{(\mu_i)}_{\mathbf{k},s}$ annihilates an electron at μ_i with momentum $\mathbf{k}$ and spin projection s. The superscript T denotes the transpose of a matrix.

SDW order with wavevector $\mathbf{Q}$ corresponds to a non-zero expectation value of the spin operator:

$$\mathbf{M} = \frac{1}{N}\sum_{\mathbf{k},ss'}\langle\Psi^{\dagger}_{\mathbf{k},s}\boldsymbol{\sigma}_{ss'}\Psi_{\mathbf{k}+\mathbf{Q},s'}\rangle, \tag{1}$$

where $\boldsymbol{\sigma}$ is the vector of Pauli matrices and N is the number of sites. Thus, $\mathbf{M}$ is a vector in spin space and a matrix in orbital space, and it modifies the electronic Hamiltonian via a Zeeman term (where g denotes the corresponding coupling constant):

$$H_Z = -g\sum_{\mathbf{k},ss'}\mathbf{M}\cdot\Psi^{\dagger}_{\mathbf{k},s}\boldsymbol{\sigma}_{ss'}\Psi_{\mathbf{k}-\mathbf{Q},s'}. \tag{2}$$

In contrast, LC order with wavevector $\mathbf{Q}$ corresponds to a non-zero expectation value of a combination of current operators, which in momentum space can be written as:

$$\Phi = \frac{1}{N}\sum_{\mathbf{k},s}\langle\Psi^{\dagger}_{\mathbf{k},s}\hat{\Gamma}_{\mathbf{k},\mathbf{k}+\mathbf{Q}}\Psi_{\mathbf{k}+\mathbf{Q},s}\rangle. \tag{3}$$

Here $\hat{\Gamma}_{\mathbf{p},\mathbf{q}}$ is an $N\times N$ matrix in orbital space that determines the real-space structure of the LCs. Time-reversal oddness of Φ requires $\hat{\Gamma}_{\mathbf{q}_1,\mathbf{q}_2} = -\hat{\Gamma}^{\mathrm{T}}_{-\mathbf{q}_2,-\mathbf{q}_1}$, assuming that time reversal does not act on μ_i.

For a kagome lattice with one orbital per site, $\hat{\Gamma}$ is a 3×3 matrix. Equivalently, in the patch description of Box 2, where $\Psi_{\mathbf{k},s} = (\psi_{\mathbf{M}_1+\mathbf{k},s}, \psi_{\mathbf{M}_2+\mathbf{k},s}, \psi_{\mathbf{M}_3+\mathbf{k},s})^{\mathrm{T}}$, LC order at wavevector $\mathbf{M}_i$ is described by $\hat{\Gamma}^{(mn)} = i\varepsilon_{lmn}$, where ε_{lmn} is the Levi-Civita symbol.

Importantly, regardless of its specific microscopic form, Φ modifies the Hamiltonian via the minimal substitution in the kinetic energy term. In a tight-binding description, it corresponds to the so-called Peierls substitution, in which the hopping parameter t_{ij} between sites i and j acquires a phase:

$$t_{ij} \to t_{ij}\exp\left(-\frac{ie}{\hbar c}\int_i^j \mathbf{A}(\mathbf{r})\cdot \mathrm{d}\mathbf{r}\right), \tag{4}$$

where $\mathbf{A}(\mathbf{r})$ is the vector potential. In the case of LCs, the relevant quantity is the flux generated by the closed loops.

For a given lattice and wavevector $\mathbf{Q}$, the LC order parameter Φ, as well as the CDW order parameter W, can be classified according to the irreducible representations (irreps) of the (para)magnetic space group at $\mathbf{Q}$, independently of the microscopic mechanism. The irreps at momentum $\mathbf{Q}$ are constructed from irreps of the little group (the crystallographic operations leaving $\mathbf{Q}$ invariant), the star of $\mathbf{Q}$ (which encodes how $\mathbf{Q}$ is connected to symmetry-equivalent momenta) and the transformation properties under time-reversal symmetry.

For the kagome lattice, the space group is $P6/mmm$. At the M point, the little group is isomorphic to the orthorhombic point group D_{2h}, which has eight one-dimensional irreps. As the star of M contains three momenta and the irreps can be even or odd under time reversal, there are eight time-reversal-even three-dimensional irreps, denoted $M_a^{\pm}$, and eight time-reversal-odd three-dimensional irreps, denoted $mM_a^{\pm}$, where $a = 1, 2, 3, 4$ and $\pm$ indicates parity under inversion.

Group theory therefore constrains the three-component CDW and LC order parameters W and Φ to transform, respectively, as one of the $M_a^{\pm}$ and $mM_a^{\pm}$ irreps. As a result, despite the large number of possible microscopic LC configurations in equation (3), there are at most eight symmetry-independent LC patterns. Which irrep is realized depends on microscopic details. For example, when both CDW and LC orders are constructed from states near the same van Hove singularities, the irreps are M_1^+ for the CDW and mM_2^+ for the LC[17]. The CDW instability could also originate from a soft phonon, in which case its irrep is set by the phonon polarization; in AV_3Sb_5, there is a soft phonon transforming as M_1^+. Once the irreps of W and Φ are identified, the Ginzburg–Landau theory of the coupled LC–CDW phases follows straightforwardly. In particular, for M_1^+ CDW and mM_2^+ LC order, the free energy admits a cubic anharmonic coupling of the form $\sum W_{i_1}\Phi_{i_2}\Phi_{i_3}$ (where i_1, i_2 and i_3 are all different), the consequences of which are discussed in the main text.

In this Perspective we draw on recent developments in kagome metals to frame key open problems and future directions in the broader problem of LC magnetism. Our focus is on LC states that are intertwined with charge density waves (CDWs) and break translational symmetry. We will start with a phenomenological discussion, followed by microscopic considerations, a discussion of ab initio methods and a brief survey of the status of LC order in the AV_3Sb_5 kagome metals[12,13]. We do not aim to review the broader literature on LC orders or their connection to high-temperature superconductors, in which the proposed LC pattern would preserve translation but break inversion symmetry (see ref. 7).

Symmetries and relationship with density wave orders

From a symmetry perspective, there is no difference between a LC state that breaks translational symmetry and a SDW—provided that spin–orbit coupling is present[14]. This does not mean, however, that these states are equivalent at the microscopic level. The SDW order parameter is associated with the expectation value of the spin operator, whereas the LC order parameter corresponds to the expectation value of the current operator (see Box 1 for details). The electronic currents form interatomic closed loops, but do not generate a net non-dissipative current, which is not allowed in a non-superconducting equilibrium state.

To further illustrate the differences between SDWs and LCs, consider their impact on the electronic states. The main effect of SDWs on the electronic Hamiltonian is to create an inhomogeneous Zeeman term. In contrast, LC order is primarily associated with the kinetic energy terms. Microscopically, the effect of LCs on the electronic states arises from the coupling between the magnetic vector potential generated by the LCs and the electronic momentum (Box 1). As a result, in a tight-binding description, LC order corresponds to a change in the phase of the hopping parameters. Indeed, LC order will often generate phases of $\pm\pi/2$ in the hopping parameters, involving neighbouring sites with potentially different orbitals.

Besides its connection to SDW order, LC order is also intimately related to another phenomenon known as CDW order. We use this term to refer to any symmetry-lowering change in the electronic charge density, regardless of its microscopic origin (for example, Fermi surface nesting or electron–phonon coupling). Such a charge variation can

https://doi.org/10.1038/s41567-026-03229-z

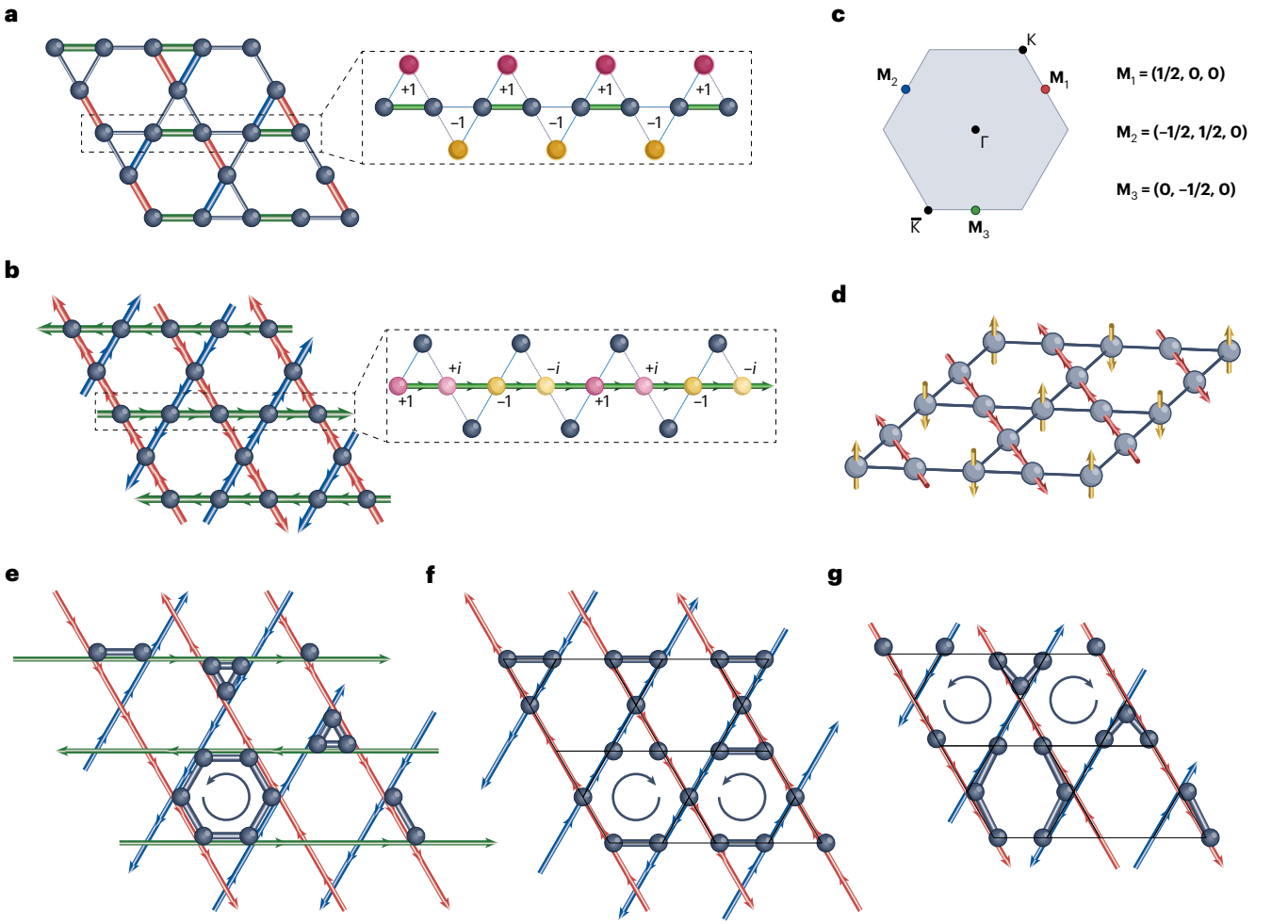


Fig. 1 | LC, CDW and SDW orders. a,**b**, Triple-**Q** CDW (**a**) and LC orders (**b**). The colours of the bonds in **a** and the currents in **b** correspond to the wavevectors in **c**. The insets in **a** and **b** show the phases $\exp(i\gamma)$ of the atomic wavefunctions for a single wavevector ($\mathbf{M}_3$). **a**, In the CDW case, the alternating phase $\gamma = 0, \pi$ corresponds to the site-CDW order (purple and yellow contours) that accompanies the bond-CDW order (green). **b**, In the LC case, the phases of the atomic wavefunctions change by $\pi/2$. **d**, LC order (red arrows) in the kagome lattice with a single wavevector ($\mathbf{M}_1$) and an SDW order with the same symmetry (yellow arrows). The spin magnetic moment vanishes on two of the sublattices. **e**–**g**, The three coupled LC–CDW phases defined in Table 1., corresponding to a 3**Q**–3**Q** phase (**e**), a 2**Q**–1**Q** phase (**f**) and a 2**Q**–3**Q** phase (**g**). The arrows show the current directions.

occur either on bonds (Schrieffer–Heeger type) or on sites (Holstein type) as shown in Fig. 1a. For simplicity, we focus hereafter on only the bond charge order.

The close connection between the LC and CDW orders stems from the fact that they modulate the phase and magnitude of the hopping parameters, respectively, as illustrated in Fig. 1a,b. For this reason, LC order that breaks translational symmetry is often referred to as an 'imaginary' CDW (denoted iCDW), and the CDW introduced above is referred to as a 'real' CDW (denoted rCDW)[15]. This nomenclature, while useful, should not be interpreted as a statement that the imaginary component of a CDW order parameter is equivalent to LC. Consider, for example, the case of a CDW wavevector that is not a time-reversal-invariant momentum, $\mathbf{Q} \neq -\mathbf{Q}$. In this situation, the CDW order parameter W, corresponding to the Fourier component of the charge density at $\mathbf{Q}$, is complex. A purely imaginary W still describes a time-reversal-symmetry-preserving charge order (corresponding to an rCDW), but it is odd under inversion. We also underline the fact that LC order is not synonymous with chiral CDW order. Chiral order means that the system lacks any improper rotations—including mirrors and inversion centres—as symmetry elements, which does not mean that the system breaks time-reversal symmetry.

Conventionally, CDW and other orders are identified by the wavevector in the Brillouin zone where the instability occurs. The most relevant points for us are the three M points located on the zone boundaries in the $q_z = 0$ plane, as shown in Fig. 1c. In the AV_3Sb_5 kagome metals, the CDW wavevector is usually at the L point, which is displaced from M along the z axis by $q_z = 1/2$. Here we simplify by focusing on CDW orders at the M point; for a detailed discussion that includes q_z effects, see refs. 16–18.

As there are three M_i points related by three-fold rotations, the CDW order parameter has three components, $W = (W_1, W_2, W_3)$, with each W_i associated with the Fourier component of the charge density at the corresponding wavevector $\mathbf{M}_i$. Given that M_i are time-reversal-invariant momenta, W_i are real-valued. The CDW free energy favours the triple-**Q** configuration $W = (W_0, W_0, \pm W_0)$, resulting in bond patterns known as star-of-David or tri-hexagonal, depending on the sign. Similarly, the LC order parameter also has three components, $\Phi = (\Phi_1, \Phi_2, \Phi_3)$, corresponding to currents flowing along different directions. The triple-**Q** LC configuration with $\Phi = (\phi_0, \phi_0, \phi_0)$ is shown in Fig. 1b, whereas Fig. 1d illustrates a single-**Q** LC configuration combined with an SDW with the same symmetry properties.

Phenomenological model of LC order

Group theory provides a useful framework for modelling the coupled CDW and LC order parameters W and Φ. As discussed in Box 1, group theory restricts the many possible bond order patterns and LC

https://doi.org/10.1038/s41567-026-03229-z

Table 1 | Common LC–CDW phases formed by different combinations of the LC and CDW order parameters. The first column corresponds to a 3Q–3Q phase; the second column, to a 2Q–1Q phase; and the third column, to a 2Q–3Q phase

LC	CDW	Magnetism	AHE/Kerr	Resistivity anisotropy	Piezomagnetism
(Φ_0, Φ_0, Φ_0)	(W_0, W_0, W_0)	Ferromagnetic	✓	×	×
$(\Phi_0, \Phi_0, 0)$	$(0, 0, W_0)$	Antiferromagnetic	×	✓	×
$(\Phi_0, 0, -\Phi_0)$	$(W_0, \tilde{W}_0, W_0)$	Ferro-octupolar	×	✓	✓

The 'Magnetism' column shows the magnetic properties of each phase and the last three columns show their experimental manifestations in terms of the anomalous Hall effect (AHE), spontaneous Kerr effect, three-fold rotational symmetry-breaking (resistivity anisotropy) and piezomagnetism.

patterns[19] to eight symmetry-distinct classes each. Moreover, group theory reveals the existence of an anharmonic LC–CDW coupling in the free energy by which the condensation of a LC order parameter with components at two distinct wavevectors, say Φ_2 and Φ_3, must trigger a CDW order-parameter component at the third wavevector, $W_1 \propto \Phi_2\Phi_3$ (refs. 17,20). In other words, a modulation of the phases of the hopping parameters typically induces a modulation in their amplitudes.

As a result of this non-trivial anharmonic coupling, the phase diagram of the coupled LC–CDW orders is very rich. Although the many independent coefficients of the Landau free energy render it challenging to make generic statements about the stable phases, it is instructive to consider the three phases shown in Table 1 and Fig. 1e–g. Other combinations of order parameters are possible, but these three flux CDW states break fewer symmetries of the parent state and often appear in phenomenological phase diagrams[17,18,20]. Note that the only phase that allows for LC order and no CDW order is the single-**Q** LC configuration $\Phi = (\Phi_0, 0, 0)$ and its symmetry-equivalent domains. In contrast, the multi-**Q** LC phases will necessarily be accompanied by CDW order.

The magnetic properties of the mixed LC–CDW phases are also rich. We illustrate this richness by discussing the properties of the three phases shown in Table 1 and Fig. 1e–g. For the 3**Q**–3**Q** configuration described by $\Phi = (\Phi_0, \Phi_0, \Phi_0)$ and $W = (W_0, W_0, W_0)$, shown in Fig. 1e (and the top row of Table 1), the magnetic moments generated by the LCs do not cancel each other exactly, resulting in a net ferromagnetic moment. The anharmonic coupling between the LC and CDW order parameters is essential for this result, as the bond distortions generated by the LCs cause the local environment experienced by the currents to become inequivalent[17]. On the other hand, as shown in Fig. 1f (middle row of Table 1), in the 2**Q**–1**Q** configuration described by $\Phi = (\Phi_0, \Phi_0, 0)$ and $W = (0, 0, W_0)$, the magnetic moments generated by the LCs cancel. This configuration has the symmetry of an antiferromagnet, in that it possesses magnetic translation symmetry. In contrast to the 3**Q**–3**Q** state, however, it breaks the six-fold rotational symmetry of the kagome lattice. Another interesting phase, displayed in Fig. 1g (bottom row of Table 1), is the 2**Q**–3**Q** state described by $\Phi = (\Phi_0, 0, -\Phi_0)$ and $W = (W_0, \tilde{W}_0, W_0)$, dubbed the congruent CDW flux phase[21]. In this case, the LC fluxes cancel, implying a vanishing net magnetic dipole moment, but the system still has a net magnetic octupole moment, which gives rise to piezomagnetism.

Microscopic mechanisms of LC order

The group theory analysis alone cannot establish which microscopic mechanisms promote this electronic instability. This requires either low-energy microscopic models of interacting electrons or ab initio calculations on materials.

Different models have been proposed to capture the M-point LC order relevant to the kagome metals. While the specific microscopic mechanisms involved in these models can vary, two common ingredients are the presence of van Hove singularities and longer-range Coulomb repulsion involving neighbouring sites[20,22–30]. To illustrate how the interplay between these two ingredients may result in a LC instability, we consider here the patch model, which focuses on the low-energy electronic states around the M points[20,31]. As discussed in Box 2, the kagome lattice generally exhibits an enhanced density of states at the M point because the electronic dispersion displays a saddle point at this momentum, as shown in Fig. 2a. In two dimensions, the density of states diverges logarithmically at the M point, resulting in a so-called van Hove singularity. Consequently, when the chemical potential is close to this van Hove singularity, small interactions can cause an electronic instability towards a symmetry-broken state.

The patch model defines three flavours of electronic states, one for each M point, as well as four symmetry-allowed interactions g_i between them, as seen in Fig. 2b. As a result of the divergent densities of states, weak coupling approaches (such as the renormalization group) can be employed. The results (details in Box 2) reveal that, depending on which of the four interactions are dominant, the resulting instability of the model is towards a LC state.

As most microscopic models rely on van Hove singularities, it is important to discuss the band structure of AV_3Sb_5. In these materials, the van Hove singularities originate from the V d orbitals[12,32]. The saddle points are close to the Fermi level on the $q_z = 0$ plane, and there is sufficient dispersion along q_z that they cross the Fermi level at non-zero q_z (refs. 33,34). Importantly, there are at least four van Hove singularities with comparable energies but different symmetries[17]. This allows extensions of the simple patch model to multi-flavour patch models, which reveal interesting new physics[26,30].

Ab initio studies on LCs, going beyond low-energy models, are rare. One exception is ref. 35, which predicted a LC phase in the absence of spin ordering in CrSi(Ge)Te_3-based systems. This scarcity may result from the fact that the commonly employed approximations to density functional theory (DFT)—the local density approximation and generalized gradient approximation—fail to capture the LC state. In these approximations, the exchange-correlation functional is spatially local, which makes them unlikely to stabilize a non-zero expectation value of the favourable interactions g_i in Fig. 2c, which have substantial intersite character. Correlated methods such as the DFT + U and DFT + dynamical mean field theory approaches[36–38], which successfully capture spin magnetism, do not usually introduce intersite exchange or correlations, and hence are not likely to reproduce LC states. A more promising approach would be to explicitly account for time-dependent processes, such as time-dependent DFT or current DFT[39–41]. However, these methods have not yet been applied to LC systems, perhaps due to the lack of reliable exchange-correlation functionals that go beyond the adiabatic local density approximation.

Experimental status in kagome metals

Determining whether LC order is realized in the AV_3Sb_5 kagome metals—and its possible type—remains a widely investigated issue. These materials display a CDW transition temperature on the order of 100 K, followed by a superconducting transition at much lower temperatures, on the order of 1 K (ref. 13). One of the pieces of evidence in favour of TRSB inside the CDW state is muon spin rotation measurements. Such measurements reveal an enhancement of the muon relaxation rate below the CDW transition, followed by another enhancement at a lower temperature, which are attributed to internal magnetic fields of ~0.01 mT arising from the electronic degrees of freedom[11,42–45]. There are also reports of a pronounced response of

https://doi.org/10.1038/s41567-026-03229-z

BOX 2

The patch model

The motivation for the patch model is that simple tight-binding models on hexagonal lattices[31] exhibit electronic dispersions with saddle points at the M points. For the kagome lattice, the dispersion near an M point takes the form:

$$E(\mathbf{k}+\mathbf{M}) \approx E_0 + \frac{\hbar^2 (k_x^2 - k_y^2)}{2m^*}, \quad (5)$$

where k_x and k_y point along the Γ–M and M–K directions, respectively, and m^* is an effective mass. Evaluation of the corresponding density of states reveals a logarithmic divergence at E_0, which is called a van Hove singularity.

The patch model (see, for example, ref. 20) focuses on the low-energy electronic state near these van Hove singularities at the M points. Such states can be expressed in terms of electron annihilation operators $\psi_{\mathbf{M}_i,s}$. An order parameter in the charge channel at momentum $\boldsymbol{M}_i = \mathbf{M}_l - \mathbf{M}_j$ for this simple case can be written as (here, i, j and k are non-repeating indices)

$$O^{\pm}_{\mathbf{M}_i} = \frac{1}{N}\sum_{\mathbf{k},s}\langle \psi^{\dagger}_{\mathbf{M}_j+\mathbf{k},s}\psi_{\mathbf{M}_l+\mathbf{k},s} \pm \psi^{\dagger}_{\mathbf{M}_l+\mathbf{k},s}\psi_{\mathbf{M}_j+\mathbf{k},s}\rangle. \quad (6)$$

The plus sign gives a real order parameter, which corresponds to the bond charge order parameter (rCDW), $O^+ \to W$. On the other hand, the minus sign gives an imaginary order parameter corresponding to the LC order parameter (iCDW), $O^- \to -i\Phi$. We emphasize that the rCDW and iCDW order parameters transform differently under time reversal, and in general have different transition temperatures.

There are four distinct types of interaction g_i involving the patch fermionic operators $\psi_{\mathbf{M}_i,s}$. Interactions g_1, g_2 and g_3 are the interpatch exchange, density–density and Umklapp interactions, respectively, whereas g_4 is the intrapatch density–density interaction, as seen in Fig. 2b. In the absence of spin–orbit coupling, there are four possible distinct density wave instabilities at $\mathbf{M}_i$, corresponding to the rCDW and iCDW and 'real' and 'imaginary' SDWs (rSDW and iSDW). The iSDW corresponds to a state with spin LCs. In the presence of spin–orbit coupling, iCDW and rSDW are symmetry-equivalent, as are the iSDW and rCDW.

The leading instability is determined by the interpatch interactions: $g_1 > 0$ favours an instability in the spin channel, whereas $g_1 < 0$ favours one in the charge channel. A value of $g_2 > 0$, on the other hand, favours both channels equally. Finally, $g_3 > 0$ favours an instability in the iCDW (or rSDW) channel over the rCDW (or iSDW) channel. Thus, the iCDW phase is expected when $g_1 < 0$, $g_2 > 0$ and $g_3 > 0$. We note that these interactions are flowing interactions in the renormalization group sense, in that they are renormalized due to the interference between different channels. In addition to these four density wave channels, the system can also be unstable towards a superconducting instability either in the conventional s-wave channel or in the unconventional $d + id$ channel[20,31].

the CDW state to a magnetic field, which is again consistent with LC order. Scanning tunnelling microscopy measurements on all three members of this kagome family showed that the relative amplitude between the CDW Bragg peaks changes sign depending on the direction of the out-of-plane applied magnetic field[21,46–48]; ref. 49, however, does not report such a behaviour. One of these studies[46] interpreted this response in terms of a chiral CDW, whereas ref. 21 attributed this behaviour to piezomagnetism, meaning a shear strain triggered by the magnetic field in linear order. Besides scanning tunnelling microscopy, transport measurements show that an in-plane resistivity anisotropy emerges inside the CDW state only when a magnetic field is applied[50], a behaviour that was also associated with the condensation of LC order[18]. Additional evidence for TRSB comes from torque magnetometry data[51] and from nonlinear transport measurements that show magnetochiral anisotropy[52], which also implies broken mirror symmetries.

Direct measurements of a magnetic moment originating from the LC order remain controversial. An anomalous Hall effect, in which the Hall conductivity retains a non-zero value after the applied field is removed and requires a non-zero net magnetization, has not been reported. Large responses of the Hall conductivity[53] and the Nernst coefficient[54] to an applied magnetic field were found, but their origins remain undetermined[55]. Moreover, spin-polarized scanning tunnelling microscopy measurements did not show evidence of magnetic moments[56]. A spontaneous Kerr effect, which requires non-zero net magnetization, was reported in refs. 57,58 below the CDW transition. However, refs. 59,60 did not observe a spontaneous Kerr effect, with the former noting instead that a strong diamagnetic contribution to the susceptibility appears below the CDW transition. A spin-polarized neutron diffraction study observed only a hint of weak magnetic scattering at the corner of the second Brillouin zone, close to the detection limit, but consistent with a moment of the order of $0.01\,\mu_B$ for each V triangle in CsV_3Sb_5 (ref. 61). A recent experiment using a tuning fork resonator reported a similarly small magnetic moment deep inside the CDW phase[62].

In interpreting these experimental results, it is important to emphasize that orbital magnetic moments are typically small and that a LC state does not necessarily induce a net magnetization, since TRSB is not synonymous with ferromagnetism. This implies that the absence of effects that require the presence of a net magnetic dipole moment, such as the spontaneous Kerr effect and the anomalous Hall effect, is not necessarily inconsistent with a LC state. Indeed, among the flux CDW states discussed in Table 1, only the $3\mathbf{Q}$–$3\mathbf{Q}$ state displays a non-zero magnetization, whereas the LC patterns of the $2\mathbf{Q}$–$1\mathbf{Q}$ and $2\mathbf{Q}$–$3\mathbf{Q}$ states break time-reversal symmetry in different ways[17]. Moreover, even if a net orbital magnetization is present on a kagome layer, it might be staggered along the c axis, as the CDW wavevector in these materials typically has a non-zero Q_z value. As for the flux CDW states that display no net magnetization on a kagome plane, while the rotational-symmetry-breaking $2\mathbf{Q}$–$1\mathbf{Q}$ state displays a flux configuration analogous to a spin antiferromagnetic phase, the $2\mathbf{Q}$–$3\mathbf{Q}$ congruent CDW flux phase displays a net magnetic octupole moment, which is manifested experimentally as piezomagnetism[21]. As pointed out in ref. 21, if the LC state is indeed piezomagnetic, residual strain can locally condense a non-zero magnetization, which could be picked up, for instance, by measurements of the Kerr effect. Moreover, while the anharmonic coupling between LC and CDW implies that LC order necessarily triggers CDW order, the converse is not necessarily true. Nevertheless, this coupling can favour the emergence of LC order inside the CDW phase[16]. Overall, it is clear that the CDW phase of the AV_3Sb_5 kagome metals displays sizable responses to magnetic fields and strain, as discussed in ref. 50. Although this makes the identification of the potential LC state challenging, it also opens the door for new physical behaviours.

Outlook

In summary, the possible realization of LCs in kagome metals provides new opportunities to elucidate and investigate this unusual type of magnetism. These include experimental probes of TRSB that do not rely solely on the existence of a net magnetization, such as piezomagnetism or magneto-electric effects. On the theory front, open challenges encompass ab initio predictions of LC order, as well as understanding its mechanisms and interplay with other electronic degrees of freedom. In particular, the interplay with charge order,

https://doi.org/10.1038/s41567-026-03229-z

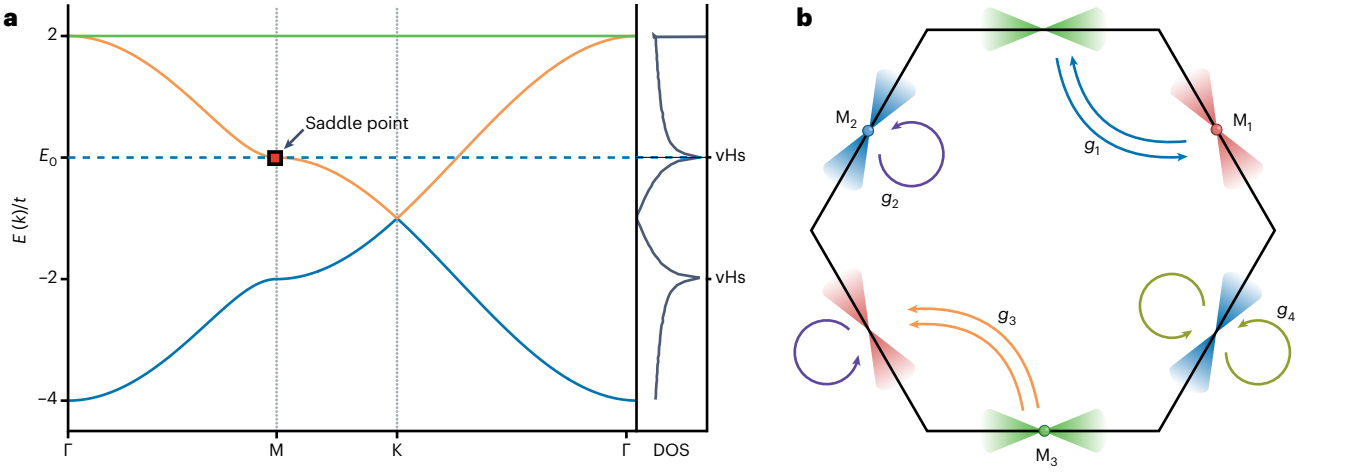


Fig. 2 | Saddle points, van Hove singularities and the patch model. a, Left: band structure of the nearest-neighbour tight-binding model on the kagome lattice, highlighting the saddle point. Right: saddle points give rise to a logarithmically diverging density of states (DOS) at the corresponding chemical potential, corresponding to a van Hove singularity (vHs). **b**, The patch model. The four different types of interaction coupling the electronic states around each M-point van Hove singularity[20] are highlighted. The arrows connect the states coupled by the interactions.

which occurs naturally in systems with three-fold rotational symmetry, is a central aspect of this state's phenomenology. The interplay with superconductivity, which is realized in kagome metals at temperatures much lower than the CDW one, also remains an open question. It has recently been shown that intra-unit-cell LC fluctuations associated with broken inversion symmetry are detrimental to pairing[63]. However, the role of LC fluctuations at finite wavevectors—such as those discussed here—in mediating superconductivity deserves further exploration. More broadly, advances in the investigation of LC in kagome metals and beyond would benefit from new experimental and theoretical approaches designed specifically to probe or model orbital magnetism, as most of the widely employed approaches to study magnetism have been developed for spin degrees of freedom. In this regard, the close connection between orbital magnetism and Berry curvature could unlock unique magnetically enabled topological properties in systems with LC order. Therefore, while the fundamental differences between spin and LC magnetism bring new challenges, they also open new avenues to explore magnetism, one of the most fascinating collective electronic phenomena realized in materials.

References

1. Hsu, T. C., Marston, J. B. & Affleck, I. Two observable features of the staggered-flux phase at nonzero doping. *Phys. Rev. B* **43**, 2866–2877 (1991).
2. Varma, C. M. Non-Fermi-liquid states and pairing instability of a general model of copper oxide metals. *Phys. Rev. B* **55**, 14554–14580 (1997).
3. Chakravarty, S., Laughlin, R. B., Morr, D. K. & Nayak, C. Hidden order in the cuprates. *Phys. Rev. B* **63**, 094503 (2001).
4. Sun, K. & Fradkin, E. Time-reversal symmetry breaking and spontaneous anomalous Hall effect in Fermi fluids. *Phys. Rev. B* **78**, 245122 (2008).
5. Venderbos, J. W. F. Symmetry analysis of translational symmetry broken density waves: application to hexagonal lattices in two dimensions. *Phys. Rev. B* **93**, 115107 (2016).
6. Haldane, F. D. M. Model for a quantum Hall effect without Landau levels: condensed-matter realization of the "parity anomaly". *Phys. Rev. Lett.* **61**, 2015–2018 (1988).
7. Bourges, P., Bounoua, D. & Sidis, Y. Loop currents in quantum matter. *C. R. Phys* **22**, 7–31 (2021).
8. Zhang, Y. et al. Control of chiral orbital currents in a colossal magnetoresistance material. *Nature* **611**, 467–472 (2022).
9. Ortiz, B. R. et al. New kagome prototype materials: discovery of KV_3Sb_5, RbV_3Sb_5, and CsV_3Sb_5. *Phys. Rev. Mater.* **3**, 094407 (2019).
10. Ortiz, B. R. et al. Superconductivity in the $\mathbb{Z}_2$ kagome metal KV_3Sb_5. *Phys. Rev. Mater.* **5**, 034801 (2021).
11. Mielke, C. et al. Time-reversal symmetry-breaking charge order in a kagome superconductor. *Nature* **602**, 245–250 (2022).
12. Neupert, T., Denner, M. M., Yin, J.-X., Thomale, R. & Hasan, M. Z. Charge order and superconductivity in kagome materials. *Nat. Phys.* **18**, 137–143 (2022).
13. Wilson, S. D. & Ortiz, B. R. AV_3Sb_5 kagome superconductors. *Nat. Rev. Mater.* **9**, 420 (2024).
14. Klug, M., Kang, J., Fernandes, R. M. & Schmalian, J. Orbital loop currents in iron-based superconductors. *Phys. Rev. B* **97**, 155130 (2018).
15. Chubukov, A. V. Renormalization group analysis of competing orders and the pairing symmetry in fe-based superconductors. *Phys. C* **469**, 640–650 (2009).
16. Christensen, M. H., Birol, T., Andersen, B. M. & Fernandes, R. M. Theory of the charge density wave in AV_3Sb_5 kagome metals. *Phys. Rev. B* **104**, 214513 (2021).
17. Christensen, M. H., Birol, T., Andersen, B. M. & Fernandes, R. M. Loop currents in AV_3Sb_5 kagome metals: multipolar and toroidal magnetic orders. *Phys. Rev. B* **106**, 144504 (2022).
18. Wagner, G., Guo, C., Moll, P. J. W., Neupert, T. & Fischer, M. H. Phenomenology of bond and flux orders in kagome metals. *Phys. Rev. B* **108**, 125136 (2023).
19. Feng, X., Zhang, Y., Jiang, K. & Hu, J. Low-energy effective theory and symmetry classification of flux phases on the kagome lattice. *Phys. Rev. B* **104**, 165136 (2021).
20. Park, T., Ye, M. & Balents, L. Electronic instabilities of kagome metals: saddle points and Landau theory. *Phys. Rev. B* **104**, 035142 (2021).
21. Xing, Y. et al. Optical manipulation of the charge-density-wave state in RbV_3Sb_5. *Nature* **631**, 60 (2024).
22. Denner, M. M., Thomale, R. & Neupert, T. Analysis of charge order in the kagome metal AV_3Sb_5 (A = K, Rb, Cs). *Phys. Rev. Lett.* **127**, 217601 (2021).
23. Tazai, R., Yamakawa, Y., Onari, S. & Kontani, H. Mechanism of exotic density-wave and beyond-Migdal unconventional superconductivity in kagome metal AV_3Sb_5 (A = K, Rb, Cs). *Sci. Adv.* **8**, eabl4108 (2022).
24. Ferrari, F., Becca, F. & Valentí, R. Charge density waves in kagome-lattice extended Hubbard models at the van Hove filling. *Phys. Rev. B* **106**, L081107 (2022).

25. Dong, J.-W., Wang, Z. & Zhou, S. Loop-current charge density wave driven by long-range Coulomb repulsion on the kagomé lattice. *Phys. Rev. B* **107**, 045127 (2023).
26. Scammell, H. D., Ingham, J., Li, T. & Sushkov, O. P. Chiral excitonic order from twofold van Hove singularities in kagome metals. *Nat. Commun.* **14**, 605 (2023).
27. Wu, Y.-M., Thomale, R. & Raghu, S. Sublattice interference promotes pair density wave order in kagome metals. *Phys. Rev. B* **108**, L081117 (2023).
28. Chen, Y., Jiang, K., Zhang, Y. & Hu, J. Flux phases in the extended Hubbard model on the triangular lattice. *Sci. China Phys. Mech. Astron.* **67**, 297211 (2024).
29. Fu, R. Q. et al. Exotic charge density waves and superconductivity on the kagome lattice. *Natl Sci. Rev.* **12**, nwaf414 (2024).
30. Li, H., Kim, Y. B. & Kee, H.-Y. Intertwined van Hove singularities as a mechanism for loop current order in kagome metals. *Phys. Rev. Lett.* **132**, 146501 (2024).
31. Lin, Y. P. & Nandkishore, R. M. Complex charge density waves at van Hove singularity on hexagonal lattices: Haldane-model phase diagram and potential realization in the kagome metals AV_3Sb_5 (*A* = K, Rb, Cs). *Phys. Rev. B* **104**, 045122 (2021).
32. Kang, M. et al. Twofold van Hove singularity and origin of charge order in topological kagome superconductor CsV_3Sb_5. *Nat. Phys.* **18**, 301–308 (2022).
33. Jeong, M. Y. et al. Crucial role of out-of-plane Sb *p* orbitals in Van Hove singularity formation and electronic correlations in the superconducting kagome metal CsV_3Sb_5. *Phys. Rev. B* **105**, 235145 (2022).
34. Ritz, E. T. et al. Superconductivity from orbital-selective electron-phonon coupling in AV_3Sb_5. *Phys. Rev. B* **108**, L100510 (2023).
35. Liu, J., Park, S. Y., Garrity, K. F. & Vanderbilt, D. Flux states and topological phases from spontaneous time-reversal symmetry breaking in CrSi(Ge)Te_3 systems. *Phys. Rev. Lett.* **117**, 257201 (2016).
36. Anisimov, V. I., Zaanen, J. & Andersen, O. K. Band theory and Mott insulators: Hubbard U instead of Stoner I. *Phys. Rev. B* **44**, 943–954 (1991).
37. Kotliar, G. et al. Electronic structure calculations with dynamical mean-field theory. *Rev. Mod. Phys.* **78**, 865–951 (2006).
38. Paul, A. & Birol, T. Applications of DFT + DMFT in materials science. *Annu. Rev. Mater. Res.* **49**, 31–52 (2019).
39. Runge, E. & Gross, E. K. U. Density-functional theory for time-dependent systems. *Phys. Rev. Lett.* **52**, 997–1000 (1984).
40. Vignale, G. & Kohn, W. Current-dependent exchange-correlation potential for dynamical linear response theory. *Phys. Rev. Lett.* **77**, 2037–2040 (1996).
41. Marques, M. A. L. et al. *Time-Dependent Density Functional Theory* Vol. 706 (Springer, 2006).
42. Yu, L. et al. Evidence of a hidden flux phase in the topological kagome metal CsV_3Sb_5. Preprint at https://arxiv.org/abs/2107.10714 (2021).
43. Khasanov, R. et al. Time-reversal symmetry broken by charge order in CsV_3Sb_5. *Phys. Rev. Res.* **4**, 023244 (2022).
44. Guguchia, Z. et al. Tunable unconventional kagome superconductivity in charge ordered RbV_3Sb_5 and KV_3Sb_5. *Nat. Commun.* **14**, 153 (2023).
45. Bonfà, P. et al. Unveiling the nature of electronic transitions in RbV_3Sb_5 with avoided level crossing μSR. *Phys. Rev. Res.* **7**, L032046 (2024).
46. Jiang, Y.-X. et al. Unconventional chiral charge order in kagome superconductor KV_3Sb_5. *Nat. Mater.* **20**, 1353–1357 (2021).
47. Shumiya, N. et al. Intrinsic nature of chiral charge order in the kagome superconductor RbV_3Sb_5. *Phys. Rev. B* **104**, 035131 (2021).
48. Deng, H. et al. Chiral kagome superconductivity modulations with residual Fermi arcs. *Nature* **632**, 775–781 (2024).
49. Candelora, C. et al. Quantifying magnetic field driven lattice distortions in kagome metals at the femtometer scale using scanning tunneling microscopy. *Phys. Rev. B* **109**, 155121 (2024).
50. Guo, C. et al. Correlated order at the tipping point in the kagome metal CsV_3Sb_5. *Nat. Phys.* **20**, 579–584 (2024).
51. Asaba, T. et al. Evidence for an odd-parity nematic phase above the charge-density-wave transition in a kagome metal. *Nat. Phys.* **20**, 40–46 (2024).
52. Guo, C. et al. Switchable chiral transport in charge-ordered kagome metal CsV_3Sb_5. *Nature* **611**, 461–466 (2022).
53. Yu, F. H. et al. Concurrence of anomalous Hall effect and charge density wave in a superconducting topological kagome metal. *Phys. Rev. B* **104**, L041103 (2021).
54. Chen, D. et al. Anomalous thermoelectric effects and quantum oscillations in the kagome metal CsV_3Sb_5. *Phys. Rev. B* **105**, L201109 (2022).
55. Koshelev, A. E., Chapai, R., Chung, D. Y., Mitchell, J. F. & Welp, U. Origin of anomalous magnetotransport in kagome superconductors AV_3Sb_5 (*A* = K,Rb,Cs). *Phys. Rev. B* **110**, 024512 (2024).
56. Li, H. et al. No observation of chiral flux current in the topological kagome metal CsV_3Sb_5. *Phys. Rev. B* **105**, 045102 (2022).
57. Xu, Y. et al. Three-state nematicity and magneto-optical Kerr effect in the charge density waves in kagome superconductors. *Nat. Phys.* **18**, 1470–1475 (2022).
58. Hu, Y. et al. Time-reversal symmetry breaking in charge density wave of CsV_3Sb_5 detected by polar Kerr effect. Preprint at https://arxiv.org/abs/2208.08036 (2022).
59. Saykin, D. R. et al. High resolution polar Kerr effect studies of CsV_3Sb_5: tests for time-reversal symmetry breaking below the charge-order transition. *Phys. Rev. Lett.* **131**, 016901 (2023).
60. Farhang, C., Wang, J., Ortiz, B. R., Wilson, S. D. & Xia, J. Unconventional specular optical rotation in the charge ordered state of kagome metal CsV_3Sb_5. *Nat. Commun.* **14**, 5326 (2023).
61. Liège, W. et al. Search for orbital magnetism in the kagome superconductor CsV_3Sb_5 using neutron diffraction. *Phys. Rev. B* **110**, 195109 (2024).
62. Gui, H. et al. Probing orbital magnetism of a kagome metal csv_3sb_5 by a tuning fork resonator. *Nat. Commun.* **16**, 4275 (2025).
63. Palle, G., Ojajärvi, R., Fernandes, R. M. & Schmalian, J. Superconductivity due to fluctuating loop currents. *Sci. Adv.* **10**, eadn3662 (2024).

Acknowledgements

We thank B. Andersen, L. Balents, M. Christensen, V. Madhavan, T. Park, E. Ritz, H. Roising, Z. Wang, S. Wilson and I. Zeljkovic for fruitful discussions. R.M.F. was supported by the Air Force Office of Scientific Research under award no. FA9550-21-1-0423. D.V. was supported by NSF grant no. DMR-2421845. T.B. was supported by the NSF CAREER grant no. DMR2046020.

Author contributions

All authors wrote the manuscript.

Competing interests

The authors declare no competing interests.

Additional information

Correspondence should be addressed to Rafael M. Fernandes, Turan Birol, Mengxing Ye or David Vanderbilt.

Peer review information *Nature Physics* thanks Dongwook Go and the other, anonymous, reviewer(s) for their contribution to the peer review of this work.

Reprints and permissions information is available at www.nature.com/reprints.

Publisher's note Springer Nature remains neutral with regard to jurisdictional claims in published maps and institutional affiliations.

Springer Nature or its licensor (e.g. a society or other partner) holds exclusive rights to this article under a publishing agreement with the author(s) or other rightsholder(s); author self-archiving of the accepted manuscript version of this article is solely governed by the terms of such publishing agreement and applicable law.

© Springer Nature Limited 2026